JACS Au
AN OPEN ACCESS JOURNAL OF THE AMERICAN CHEMICAL SOCIETY

pubs.acs.org/jacsau
Article

Computation-Aided Development of Next-Generation Extractants for Trivalent Actinide and Lanthanide Separation

Xiaofan Yang,[#] Dong Fang,[#] Linjia Chen,[#] Yaoyang Liu, Shihui Wang, Lei Xu, Anyun Zhang, Jing Su,* Chao Xu,* and Chengliang Xiao*

Cite This: *JACS Au* 2024, 4, 4744−4756
Read Online
ACCESS | Metrics & More | Article Recommendations | Supporting Information

ABSTRACT: The chemical similarities between trivalent actinides [An(III)] and lanthanides [Ln(III)] present a significant challenge in differentiating and separating them, which is a key step toward closing the nuclear fuel cycle. However, the existing separation approaches commonly suffer from demerits such as inadequate separation factors, limited stripping efficiency, and undesired coextraction. In this study, a novel unsymmetrical phenanthroline-derived amide-triazine (Et-Tol-CyMe$_4$-ATPhen) extractant was first designed and then screened with theoretical computation. Meanwhile, they were successfully synthesized by using a *de novo* construction method. As expected, Et-Tol-CyMe$_4$-ATPhen exhibited a favorable extraction ability for Am(III) and minimal extraction for Ln(III), thereby achieving an extremely selective An(III)/Ln(III) separation with a separation factor of over 280. Furthermore, Am(III) could be easily and effectively stripped from the loaded phases using dilute nitric acid. The underlying coordination mechanisms were thoroughly elucidated by using ^{1}H NMR, ESI-MS, UV−vis absorption spectrometry, photoluminescence spectrometry, and single-crystal X-ray diffraction. This work holds promise for addressing the current challenges in An(III)/Ln(III) separation and represents a pioneering endeavor in developing next-generation extractants from first-principles calculation.

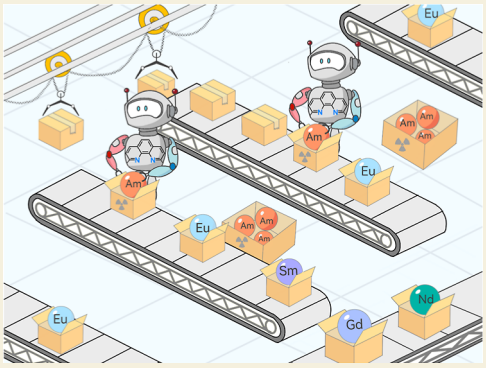

KEYWORDS: *actinides, lanthanides, selective separation, computational-aided, complexation mechanism*

1. INTRODUCTION

Lanthanides and actinides, defined by 4f and 5f electrons, compose the f-block elements.[1] The lanthanide series spans La to Lu and exists primarily as stable Ln(III) ions in aqueous solution.[2] Among the actinides, Th, U, Np, and Pu commonly show oxidation states of +4, +6, +5, and +4 in the aqueous phase, respectively.[3] Other actinides mainly exist as An(III) ions under acidic conditions.[4] Minor actinides like americium (Am) and curium (*Cm*) are produced in nuclear reactors from neutron capture of uranium.[5] Recovering minor actinides from spent nuclear fuel for recycling or transmutation aligns with environmental protection and nuclear safety imperatives.[6,7] Lanthanides are high neutron-capture fission products (e.g., ^{149}Sm and ^{157}Gd), and their coexistence with minor actinides will severely hinder efficient transmutation and utilization of the 5f nuclides, emphasizing the need for effective separation of the two groups of elements.[8] However, efficient separation of An(III)/Ln(III), especially via the industrially favorable solvent extraction technique remains a great challenge,[9,10] which stems from nearly identical chemical behaviors between An(III) and Ln(III) in terms of closely similar outer electronic configurations, same valence states, and comparable ionic radii.[11] According to the hard−soft acid-base (HSAB) theory, An(III) species with more diffuse 5f electron orbitals exhibit softer acid character as compared to their 4f Ln(III) counterparts.[12,13] Therefore, An(III) ions show a stronger affinity toward soft donor bases like N or S, rationalizing the employment of lipophilic extractants with N or S donor atoms for An(III)/Ln(III) separation.[14]

There were no extractants capable of separating trivalent actinides and lanthanides under highly acidic conditions until 2,6-bis(1,2,4-triazin-3-yl)pyridine (BTP) ligands were discovered.[15] However, BTP's stability under strong acidity and irradiation was proven unsatisfactory.[16] A promising tetradentate 6,6′-bis(1,2,4-triazin-3-yl)-2,2′-bipyridine ligand (BTBP) was then found to show robust Am(III)/Eu(III) separation in low-polarity solvents.[17] Yet, the slow extraction kinetics resulting from the rotatable bipyridine skeleton of BTBP necessitated the addition of malonamide ligands to facilitate the metal transfer from the aqueous solution to the organic phase.[18] Further modification led to a rigid 2,9-bis(1,2,4-triazin-

Received: July 30, 2024
Revised: September 11, 2024
Accepted: September 16, 2024
Published: September 23, 2024

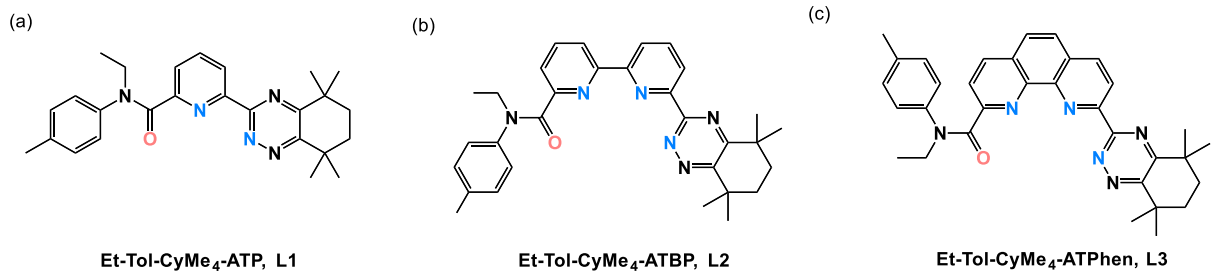

Figure 1. Three extractants designed and developed in this work. (a) Et-Tol-CyMe$_4$-ATP, **L1**; (b) Et-Tol-CyMe$_4$-ATBP, **L2**; (c) Et-Tol-CyMe$_4$-ATPhen, **L3**.

3-yl)-1,10-phenanthroline (BTPhen) extractant with expedited kinetics and improved extraction capability,[19] but the coextraction with Ln(III) and extremely high affinity to Am(III) posed stripping challenges.[20] Coordination chemistry experiments in solution and solid systems confirmed that 1,10-phenanthroline-2,9-dicarboxamide (PDAM) held a strong affinity to Ln(III) ions with large radii and it may have potential An(III)/Ln(III) separation ability.[21,22]

Therefore, the *N*,*O*-hybrid *N*,*N*′-diethyl-*N*,*N*′-ditolyl-2,9-diamide-1,10-phenanthroline (Et-Tol-DAPhen) extractant was developed by combining soft N donor atoms on the phenanthroline skeleton and hard O donor atoms on amide side chains, and this ligand exhibited a notable An(III/IV/VI)/Eu(III) separation efficacy.[23−25] However, the cascade countercurrent extraction test revealed a periodic trend in Et-Tol-DAPhen's extraction efficiency for Ln(III) with a significant coextraction phenomenon observed for light lanthanides.[26] Meanwhile, a class of bis-lactam-1,10-phenanthroline (BLPhen) extractants have been developed through preorganized modification and they exhibited enhanced Am(III) extraction capability.[27,28] However, under highly acidic conditions, noticeable coextraction of Ln(III) ions was also observed.[29]

At present, rarely reported extractants could simultaneously combine the advantages of strong extraction ability in high acidity, complete separation ability for Am(III)/Ln(III), and convenient stripping (Appendix A in the Supporting Information).[30−32] Meanwhile, conventional synthesis methods for phenanthroline-derived extractants were usually based on direct grafting of side functional groups onto the phenanthroline skeleton, causing difficulties in modification and limiting the finding of novel structures.[33,34] Based on the summary and comparison of the extractants mentioned above, we believe that the ideal An(III)/Ln(III) extractant is an asymmetric extractant composed of an *N*-heterocyclic skeleton, amide, and triazine side chains.[35] The selection of *N*-heterocyclic molecules (such as pyridine, bipyridine, and phenanthrene) as the extractant skeleton can ensure the extraction separation ability under highly acidic conditions. The amide side chain with an O donor atom can improve the extraction and stripping ability of actinides, while the triazine side chain with a N donor atom can improve the selectivity of Am(III) over Eu(III).

Numerous studies have shown that density functional theory (DFT) calculations can predict the An(III)/Ln(III) separation trend observed in experiments and provide an in-depth understanding of the extraction and separation mechanisms.[36−40] This emphasizes the reliability of DFT calculations in exploring the extraction and separation capabilities of extractants. In addition, as compared to experimental methodologies, DFT calculations required less manpower, budget, and time, thus allowing for more efficient screening of extractant structures and enabling rapid optimization.[41−43] Consequently, DFT calculations have become an important tool in the research of An(III)/Ln(III) separation processes.[44,45]

Herein, we designed three unsymmetrical extractants (2-*N*-ethyl-*N*-(tolyl)carboxamide-6-(5,5,8,8-tetramethylcyclohexyl-[1,2,4]triazin-3-yl)-pyridine) (Et-Tol-CyMe$_4$-ATP, **L1**, Figure 1a), 6-*N*-ethyl-*N*-(tolyl)carboxamide-6′-(5,5,8,8-tetramethylcyclohexyl-[1,2,4]triazin-3-yl)-2,2′-bipyridine (Et-Tol-CyMe$_4$-ATBP, **L2**, Figure 1b), and 2-*N*-ethyl-*N*-(tolyl)carboxamide-9-(5,5,8,8-tetramethylcyclohexyl-[1,2,4]triazin-3-yl)-1,10-phenanthroline (Et-Tol-CyMe$_4$-ATPhen, **L3**, Figure 1c) by incorporating both amide and triazine functional groups onto the *N*-heterocyclic skeletons. The DFT screening results suggested that **L3** was the optimal extractant. A brand-new *de novo* construction method was then developed to successfully synthesize this phenanthroline-derived **L3** extractant. Subsequent solvent extraction results confirmed the DFT predictions, highlighting **L3**'s favorable extraction for Am(III) and its convenient stripping. Furthermore, **L3** showed a weak extraction toward all the Ln(III) ions, achieving a notable An(III)/Ln(III) separation. The coordination mechanisms of **L3** with f-block elements were fully disclosed via various spectroscopic methods and structural characterizations. This study provided an innovative unsymmetrical phenanthroline-derived extractant of great potential in solving the current challenges in An(III)/Ln(III) separation.

2. METHODS

2.1. DFT Computational Details

Kohn−Sham DFT calculations were performed on the following molecules: **L1**, **L2**, **L3**, ML(NO$_3$)$_3$ [M = Am(III), Eu(III); L = 1,2,3] and [M(**L3**)$_2$NO$_3$]$^{2+}$ [M = Am(III), Eu(III)].[46,47] Geometry optimizations were performed by employing the hybrid functional PBE0 as implemented in the Gaussian 16 program.[48,49] For Eu(III) and Am(III), the ECP28MWB/ECP28MWB-SEG[50,51] and ECP60MWB/ECP60MWB-SEG[52,53] basis sets and pseudopotentials were applied, respectively. For nonmetal atoms, the def2-TZVP basis sets[54] (**L** and ML-type complexes) and the 6-311G* basis sets[55] (ML$_2$-type complexes) were applied, respectively.

For each molecule, solvation effects were evaluated using the SMD solvation model with def2-TZVP basis sets for nonmetals and previously mentioned pseudopotentials and basis sets for metals at the DFT/PBE0 level of theory.[56] Furthermore, time-dependent density functional theory (TDDFT) calculations with the PBE0 functional (TDDFT/PBE0) were performed on **L3**, M(**L3**)(NO$_3$)$_3$, and [M(**L3**)$_2$NO$_3$]$^{2+}$ [M = Am(III), Eu(III)] using 6-311G* basis sets for nonmetals.

The chemical bonding analysis of ML(NO$_3$)$_3$ complexes, including bond order analyses,[57−59] energy decomposition analysis (EDA),[60−62] and natural orbitals for chemical valence (NOCV)[63] were performed at the above optimized geometries using the PBE functional,[64] scalar relativistic ZORA Hamiltonian,[65] and uncontracted slater-type orbital

https://doi.org/10.1021/jacsau.4c00684
JACS Au 2024, 4, 4744−4756

basis sets with the quality of triple-ζ plus two polarization functions (TZ2P)[66] implemented in the Amsterdam Density Functional (ADF 2020.103).[67,68] To balance computational accuracy and computational cost, small-core TZ2P basis sets were employed for all atoms in the bond order calculations, with the frozen core approximation applied to the inner shells $[1s^2 - 4f^{14}]$ for Am(III), $[1s^2 - 4d^{10}]$ for Eu(III), and $[1s^2]$ for C, N, and O. In the EDA calculations, all-electron TZ2P basis sets were used for all atoms.

These functionals and basis sets have been extensively tested for actinide coordination systems and shown to give good agreement with experimental data.[36,41,69,70]

2.2. Solvent Extraction and Stripping Experiments

Caution: it should be noted that ^{241}Am(III) and ^{152,154}Eu(III) both have strong radioactive and physiological toxicity. Relevant experiments were carried out in the radiochemistry laboratory at Tsinghua University.

The Am(III) feed liquid in the radioactive experiment was ^{241}Am-(III), and the Eu(III) feed liquid was a mixture of ^{152}Eu(III) and ^{154}Eu(III). First, the extractants were dissolved in 1-(trifluoromethyl)-3-nitrobenzene to prepare a solution with a concentration of 2−20 mM as the organic phase in the extraction. The radioactive elements Am(III) and Eu(III) (1.2×10^3 and 2×10^3 Bq/mL) or nonradioactive lanthanide nitrates (0.1 mM) were added to the nitric acid solution with a concentration of 0.1−4.0 M as the aqueous phase in the extraction. During the extraction experiment, 1 mL of the aqueous phase and organic phase were added to the centrifuge tube, and magnetic stirrers were used to fully mix the two phases (300 rpm, 60 min). After the extraction reached the equilibrium state, the mixture was centrifuged for phase separation (3000 rpm for 3 min). In the radioactive extraction experiment, 100 μL of aqueous-phase solutions containing Am(III) and Eu(III) were added to the liquid scintillation (LSC) bottle with LSC cocktail (Ultimate gold, PerkinElmer) and mixed intensively. The radioactive activity of Am(III) and Eu(III) in the aqueous phase before and after extraction was measured by an ultralow-level scintillation counter (Quantulus 1220, PerkinElmer). ICP-OES (iCAP-PRO, Thermo Scientific) was used to measure the concentration of Ln(III) in the aqueous phase before and after extraction. The calculation methods of the distribution ratio (D) and extraction efficiency (E) to Am(III)/Eu(III) and Ln(III) are shown in eqs S1 and S2. The slope analysis method was used to identify the chemical composition of extracted complexes, and the corresponding calculation equations are shown in eqs S4−S9.

The aqueous solutions of 0.1, 0.01, and 0.001 M HNO_3 were selected as the stripping agents. The acidity of the Am(III) feed liquid was 3 M HNO_3. The concentration of the **L3** extractant in the organic phase was 20 mM. First, the organic phases and aqueous liquids were allowed to make full contact to achieve extraction equilibrium. Then, the extracted organic phases and fresh stripping agents were mixed and centrifuged. The extracted organic phase was stripped three times by fresh stripping agents. The volume of organic and aqueous phases was equal in each extraction and stripping step. The stirring and centrifugation times were 60 and 3 min, respectively. Based on the measured radioactivity of Am(III) in the feed liquid, extracted organic phase, and stripped aqueous phase, the single and total stripping efficiencies (S %) were calculated, respectively, and the calculation method is presented in eq S3.

2.3. ^{1}H NMR Titration

CD_3OD with 99.8% deuteration and containing 0.03% (v/v) tetramethyl silane (TMS) was used as a solvent in NMR titration. The stock solutions were prepared by dissolving **L3** at a concentration of 10 mM, respectively. La(III) and Lu(III) nitrate were also prepared with a concentration of 50 mM as the titrant solution, respectively. The nuclear magnetic tube initially contained 0.5 mL of the ligand solutions, and 10 μL of metal ion stock solution was added in a single drop. The nuclear magnetic tube was oscillated (600 rpm, 3 min) to reach coordination equilibrium and obtain ^{1}H NMR spectra (AVANCE NEO 500, Bruker). The addition of metal ions was stopped after no changes were found in the NMR spectra (M/L = 2.0).

2.4. ESI-MS

Eu(III) nitrates and **L3** were dissolved in HPLC-grade acetonitrile at a concentration of around 1.0 mM as the original stock solutions. The stock solutions of ligands and metal ions were mixed in equal volumes, and sodium nitrate was added to the mixture to promote the coordination reaction. The mixtures were shaken for 3 min to ensure that the coordination reaction reached equilibrium and diluted to 0.1 mM before mass spectrometric analysis. The high-resolution mass spectrum results were obtained by a mass spectrometer (Q-TOF 6545, Agilent) without liquid chromatography separation.

2.5. UV−Vis Spectroscopic Titration

Acetonitrile with HPLC purity was used as a solvent in the UV−vis spectroscopy titration. For Eu(III)-**L3** titration. **L3** with a concentration of 0.03 mM was used as the initial titrated solution. Eu(III) nitrate with a concentration of 1.0 mM was prepared as the initial titrating solution of the metal ions. The ionic strength in Eu(III)-**L3** titration samples was controlled at 10.0 mM by $Et_4N{\cdot}NO_3$. The complexation between ligands and metal ions reached equilibrium after stirring (600 rpm, 3 min). The UV−vis titration spectra of Eu(III)-**L3** (range = 240−450 nm, step = 0.2 nm) were collected on a UV−vis−NIR spectrophotometer (Cary 5000, Agilent). The *HyperSpec* program was used to fit the stability constants (log β), molar absorptivities, and species fraction curves of ligands and complexes.[71]

2.6. Photoluminescence Titration

The stock solutions of 1.0 mM ligand and 0.1 mM Eu(III) nitrate in CH_3CN were used in photoluminescence titration experiments. Tetraethylammonium nitrate (10 mM) was added to the solutions to keep the ionic strength constant. The Eu(III) nitrate solution with an initial volume of 2.0 mL was put in a quartz cuvette with an optical path of 1 cm. After each addition, samples needed to be mixed by magnetic stirring (600 rpm, 3 min) to reach the complexation equilibrium. The titration was stopped until no significant changes were found in the photoluminescence emission spectra. The photoluminescence emission spectra with a wavelength ranging from 550 to 750 nm (step = 1 nm) were obtained by a photoluminescence spectrometer (FLS1000, Edinburgh) with the excitation wavelength set at λex = 356 nm.

2.7. Single-Crystal X-ray Diffraction

Single crystals of the **L3** ligand were obtained by cooling crystallization. By heating and stirring, a certain amount of **L3** was dissolved in acetonitrile and concentrated into a supersaturated solution with a concentration of 50 mM. Then it was left at room temperature for more than 48 h, and high-quality single crystals precipitated at the bottom of the glass bottle. The single crystal of the complex formed by Eu(III) and the **L3** ligand was obtained by the solvent diffusion method. Eu(III) nitrate (0.01 mM) was dissolved in acetonitrile with an equal amount of **L3** ligand and then placed in an ethyl ether atmosphere for diffusion. After some time (1−7 days), single crystals of the 1:1 complex precipitated from the bottom of the glass bottle. Using Eu(III) perchlorate and a double equivalent amount of the ligand, the single crystals of the 1:2 complex were obtained by the same method.

3. RESULTS AND DISCUSSION

3.1. Theoretical Prediction and Screening

The design of extractants that combine all of the merits of extraction, stripping, and selective properties for An(III)/Ln(III) separation remains a big challenge. We suppose that the unsymmetrical extractants composed of both amide and triazine functional groups onto *N*-heterocyclic skeletons (pyridine, bipyridine, and phenanthroline) could achieve this target. To rapidly validate our ideas, we decided to initially use DFT calculations to screen these three extractants based on the established application of DFT in computationally predicting the separation efficiency of extractants.

To predict the extraction and separation capabilities of the assumed ligands for Am(III) and Eu(III), DFT calculations

https://doi.org/10.1021/jacsau.4c00684
JACS Au 2024, 4, 4744−4756

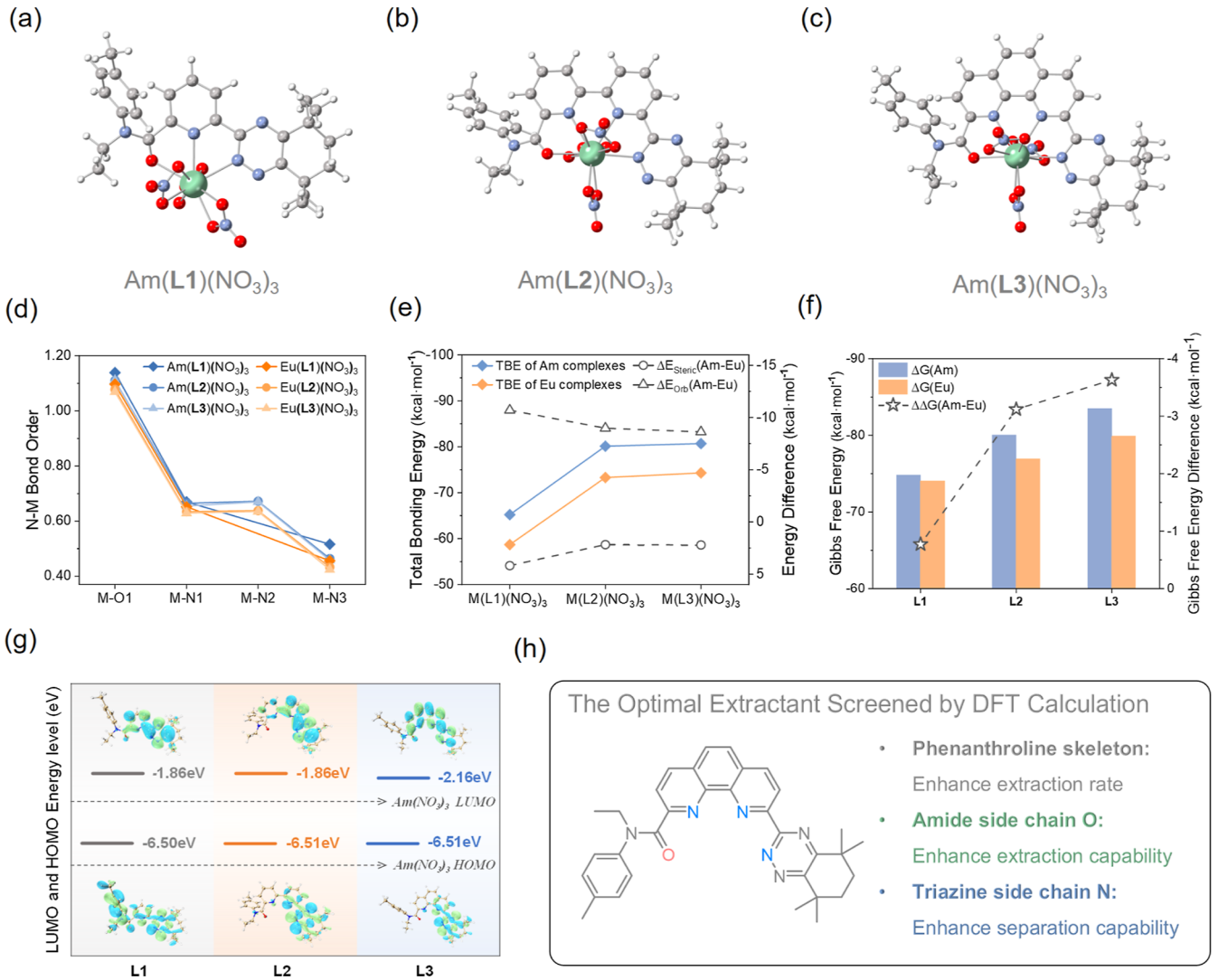

Figure 2. Optimized structures of (a) Am(**L1**)$(NO_3)_3$, (b) Am(**L2**)$(NO_3)_3$, and (c) Am(**L3**)$(NO_3)_3$. (d) Nalewajski−Mrozek (N−M) bond order analysis of ML$(NO_3)_3$ [M = Am(III), Eu(III); L = **L1**, **L2**, **L3**]. (e) EDA of the total bonding interaction between fragments M$(NO_3)_3$ and ligand in ML$(NO_3)_3$ [M = Am(III), Eu(III); L = **L1**, **L2**, **L3**]. (f) Calculated Gibbs free energies (ΔG) of the complexation reactions and the difference in ΔG between Am(III) and Eu(III) ($\Delta\Delta G$) in nitrobenzene. (g) Frontier molecular orbital energy level diagram of **L1**, **L2**, and **L3** fragments in Am(**L**)$(NO_3)_3$. The envelope of HOMO and LUMO is given with contour values of 0.02 au. (h) Design strategy of the optimal extractant screened by DFT calculation.

were first performed on the ML-type complexes, i.e., ML$(NO_3)_3$ [M = Am(III), Eu(III); **L** = **L1**, **L2**, **L3**]. Considering the rotation of the C−N single bond in the amide side chain of the ligand, our calculations considered two isomers, labeled as *is1* and *is2* (Figure S2). According to their relative energies after optimization (Figures S3 and S4 and Tables S1 and S2), *is1* was identified as the most stable one for the ML$(NO_3)_3$ complex and was employed for subsequent calculations and discussion. For all ML$(NO_3)_3$-*is1* complexes, the ligand provided three (**L1**) or four (**L2** and **L3**) coordinating atoms, along with three nitrate ions coordinating in a bidentate manner, resulting in a coordination number of 9 (**L1**) or 10 (**L2** and **L3**) for the metal center (Figure 2a−c).

To evaluate the differences in M−L chemical bonding between Am(III) and Eu(III) for each ligand and deeply explore the nature of these bonds, we performed a detailed bonding analysis on the ML$(NO_3)_3$ complex, including bond orders, EDA, and NOCV. The calculations are summarized in Tables S3−S5 and Figures S5−S16.

The results of the bond order analysis show that the bond orders for M−O and M−N with Am(III) are greater than those with Eu(III) among the three ligands (Figure 2d and Table S4). This means that the bonding interactions of the ligands with Am(III) are stronger than those with Eu(III). This difference in bonding interactions enables the ligands to have selectivity for Am(III) over Eu(III). Moreover, the EDA results (Figure 2e) show that the Am(III) complexes have more negative total bonding energies than the Eu(III) complexes, which also indicates a stronger binding affinity of these ligands toward Am(III). To further explore the driving forces behind these differences, we have compared the various components in the EDA results (Table S5). The detailed analysis reveals that the Am(III) complexes are more favorable in terms of electrostatic stabilization compared to the Eu(III) complexes. However, this interaction is offset by Pauli's repulsion energies. Hence, summing these two energies (steric interaction) resulted in small negative values (ranging from −0.44 to −7.03 kcal·mol^{-1}) for all the complexes, with more negative values observed in the

https://doi.org/10.1021/jacsau.4c00684
JACS Au 2024, 4, 4744−4756

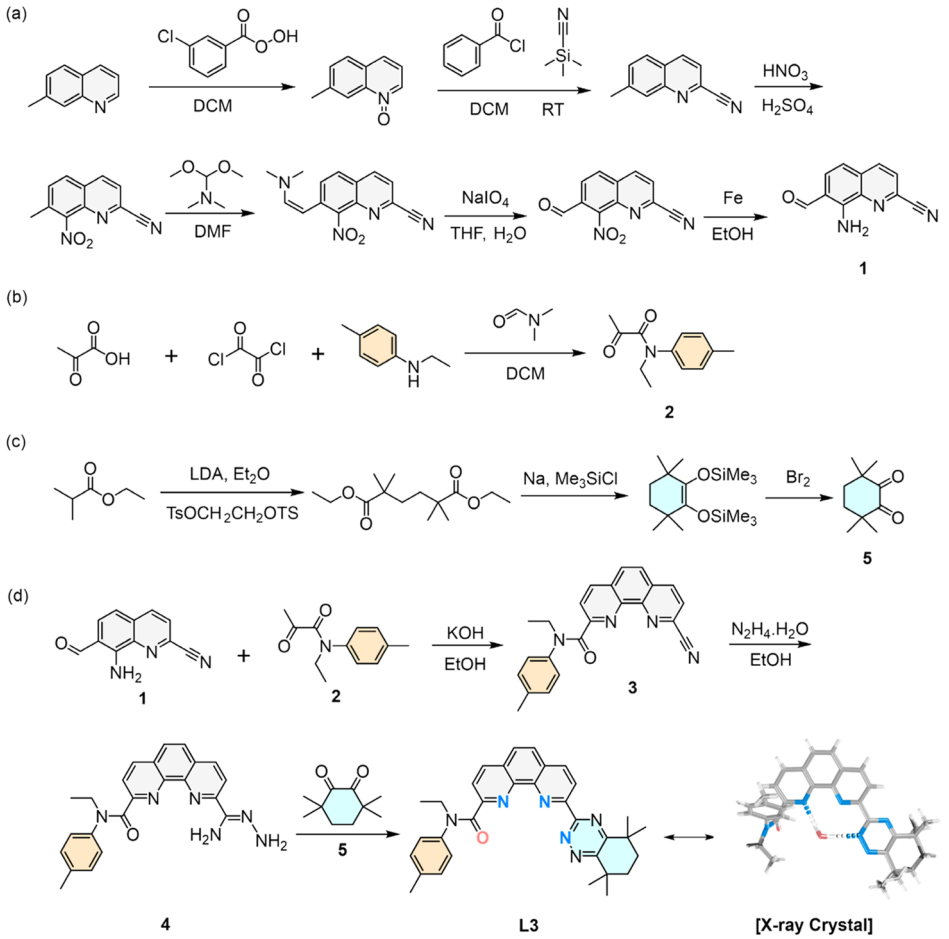

Figure 3. Synthesis methods of (a) intermediate **1**, (b) intermediate **2**, (c) intermediate **5**, and (d) **L3** extractant.

Eu(III) complexes. Considering only these two metrics, we would predict that the Am(III) complexes would not be stable compared to the Eu(III) complexes. Nevertheless, significant negative stabilization energies are obtained once the orbital interaction terms are considered. Therefore, the stronger metal−ligand orbital interactions in Am(III) complexes than those in Eu(III) complexes are regarded as the main factor in promoting ligand selectivity for Am(III) over Eu(III).

Subsequently, to further understand the orbital interactions in the complexes, we analyzed the M−O and M−N bonding interactions using the ETS-NOCV method (Figures S5−S16). The NOCV deformation densities show that the interactions between the metals and the ligands in all of the complexes are dominated by σ-bonds. These σ-bonding interactions primarily consisted of O 2p- orbitals and N 2p- orbitals mixing with 4f-/5f-, 5d-/6d-, and 6s-/7s- orbitals of the metals. As compared to the f (4f/5f) orbitals, the d (5d/6d) orbitals contribute more to metal−ligand bonding. Consistent with the results of the literature, the d orbitals are more diffuse as compared to the more contracted f orbitals, resulting in different bonding capabilities.[69,72−77]

In general, the bonding analysis of $ML(NO_3)_3$ complexes reveals that the three ligands have a stronger binding affinity to Am(III) as compared to Eu(III), suggesting that all these designed ligands may possess certain separation capabilities toward Am(III) and Eu(III). It is worth mentioning that within the same metal complex, the larger bond orders of M−O as compared to M−N also suggest that introducing O coordination can enhance the extraction capability of the ligand, which is consistent with the widely reported results in experiments.

In order to identify the most promising extractants for separating Am(III) and Eu(III), thermodynamic calculations were performed on the ML-type complexes by model reaction 1, which was generally employed in the literature.

$$[M(NO_3)(H_2O)_8]^{2+} + L + 2NO_3^- = ML(NO_3)_3 + 8H_2O \quad (1)$$

Based on the most stable conformations of the complexes (*is1*) and ligands (*C1*) (Figure S17 and Table S6), we calculated the Gibbs free energies (ΔG) of the reactions and the difference in ΔG between Am(III) and Eu(III) ($\Delta\Delta G$) (Figure 2f and Table S7). The calculated Gibbs free energies (ΔG) show that the extraction capabilities of the three ligands for the metals Am(III) and Eu(III) are **L3** > **L2** > **L1**. Additionally, the calculated $\Delta\Delta G$ values of −0.77, −3.12, and −3.73 kcal·mol^{-1} for **L1**, **L2**, and **L3**, respectively, also indicate that their separation capabilities follow the same order: **L3** > **L2** > **L1**. Ultimately, frontier molecular orbitals, the highest occupied molecular orbital (HOMO) and lowest unoccupied molecular orbital (LUMO), of ligand fragments in the complexes were analyzed (Figures 2g and S18). The results indicate that the frontier molecular orbital energies of the **L1** and **L2** fragments are quite similar. However, compared to **L1** and **L2**, **L3** exhibits a significantly lower LUMO energy level, making it easier to accept electrons from the metals. As such, **L3** is preliminarily

https://doi.org/10.1021/jacsau.4c00684
JACS Au 2024, 4, 4744−4756

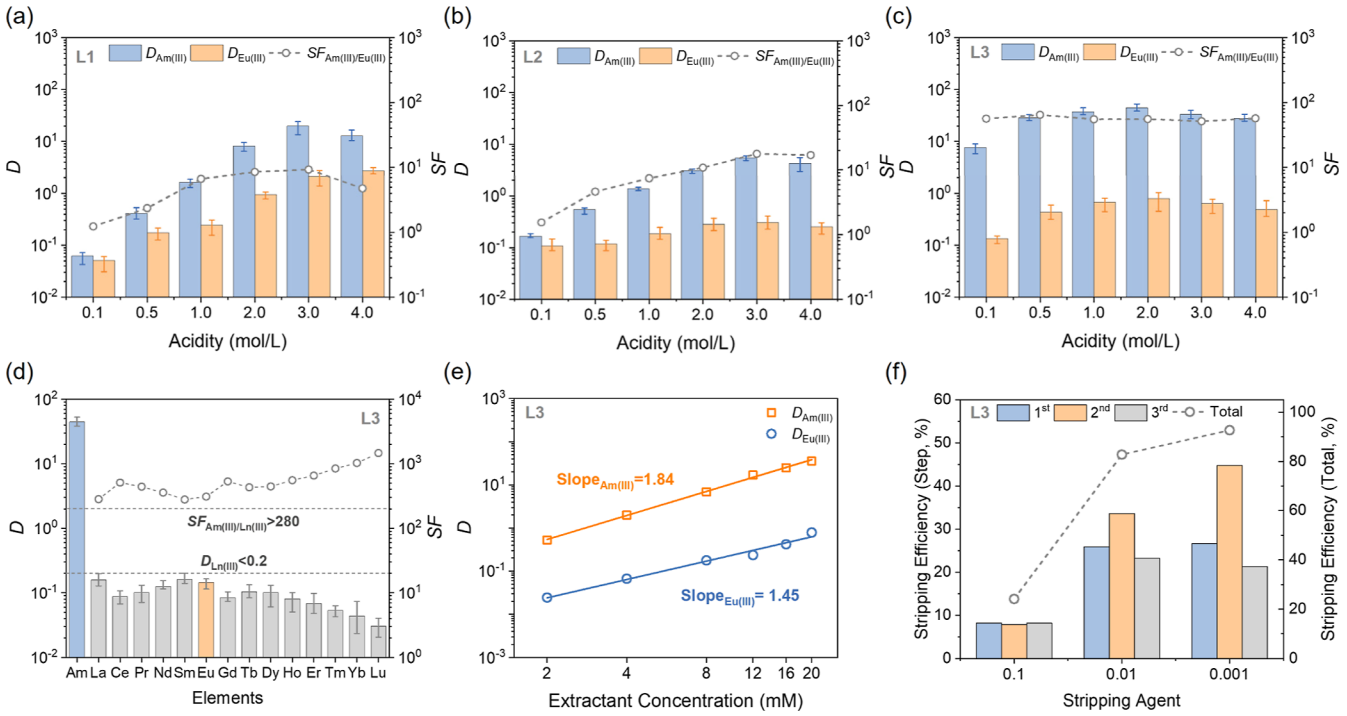

Figure 4. Influence of solution acidity ([HNO_3] = 0.1−4.0 M, [L] = 20 mM) on ^{241}Am(III)/^{152,154}Eu(III) extraction by (a) **L1**, (b) **L2**, and (c) **L3**; (d) distribution ratio of ^{241}Am(III) and Ln(III) extracted by **L3** (Ln(III) = 0.1 mM, [HNO_3] = 2.0 M, [L] = 20 mM); (e) influence of extractant concentration ([L] = 2−20 mM, 3 M HNO_3) on ^{241}Am(III)/^{152,154}Eu(III) extraction by **L3**; (f) Am(III) stripping efficiency by dilute nitric acid for **L3**.

identified as the most promising ligand for the separation of Am(III) from Eu(III).

The theoretical studies presented above predicted the extraction and separation capabilities of the three designed ligands, with the computational results all indicating that **L3** has the strongest extraction and separation capabilities. This allows us to preliminarily predict that **L3** could potentially be a promising extractant for separating Am(III) and Eu(III) (Figure 2h). However, it should be noted that although our computational method is rational and the calculation process has been thoroughly considered to enhance the reliability of the predictions, our model still involves some simplifications compared with the complex extraction systems used in experiments. Moreover, we only use the thermodynamic data of ML-type complexes to evaluate the extractants' separation capabilities, which inevitably introduces some errors. In actual extraction systems, other types of complexes, such as ML_2 or ML_3, might exist and could play a dominant role during the extraction process. Seeking experimental validation for the theoretical predictions, we subsequently synthesized **L3**, along with **L1** and **L2** for comparison, and carried out extraction experiments to confirm the critical role of computational insights in advancing separation chemistry.

3.2. Synthesis of Extractants via a *De Novo* Construction Method

The synthesis procedures of intermediate **1** (8-amino-7-formylquinoline-2-carbonitrile), intermediate **2** (*N*-ethyl-2-oxo-*N*-(*p*-tolyl)propanamide), intermediate **5** (3,3,6,6-tetramethylcyclohexane-1,2-dione), and the **L3** extractant are shown in Figure 3. The synthesis procedures of extractants **L1** and **L2** for comparison are shown in Figure S1. The ^{1}H and ^{13}C NMR spectra of the intermediates **1**, **2**, and **5** are shown in Figures S19−S24. The ^{1}H NMR, ^{1}H−^{1}H COSY, and NOESY NMR spectra, ESI-MS results, and organic elements analysis results of **L1**, **L2**, and **L3** extractants are shown in Figures S25−S31 and Table S8.

Using 7-methylquinoline as the starting material, acyl and amino groups can be introduced at positions 7 and 8 in intermediate **1** through multiple steps of substitution, oxidation, and reduction reactions. These two functional groups could provide coupling sites for the subsequent construction of the phenanthroline skeleton. Simultaneously, the carbonitrile group at position 2 serves as a reaction site for the subsequent generation of diamide dihydrazide and further cyclization reactions to form triazine side chains. The raw materials with a simple structure (pyruvate, oxalyl chloride, and *N*-ethyl-4-methylaniline) were dissolved and mixed to obtain intermediate **2** under mild conditions (room temperature) with a yield of 63%. The synthesis method of intermediate **5** can be referred from previous literature.[19] By strictly controlling reaction conditions and manipulation, we succeeded in obtaining the products with a higher yield than that reported in the literature.[19]

In the synthesis of the **L3** extractant, we abandoned the conventional strategy of functionalizing substituents directly onto the phenanthroline framework and instead pioneered a *de novo* construction of the phenanthroline skeleton based on the Friedländer reaction, achieving a high yield of 76%.[78] Furthermore, since intermediate **2** was synthesized beforehand, the amide side chain was successfully linked to the phenanthroline skeleton, thereby avoiding additional experimental steps. Additionally, the subsequent triazine cyclization reaction conditions were relatively mild and did not involve strong acids or metal catalysts, preventing hydrolysis of the amide side chain.

To date, most phenanthroline derivative extractants were synthesized by grafting the functional groups directly onto the parent phenanthroline skeleton. However, there are apparent

https://doi.org/10.1021/jacsau.4c00684
JACS Au 2024, 4, 4744−4756

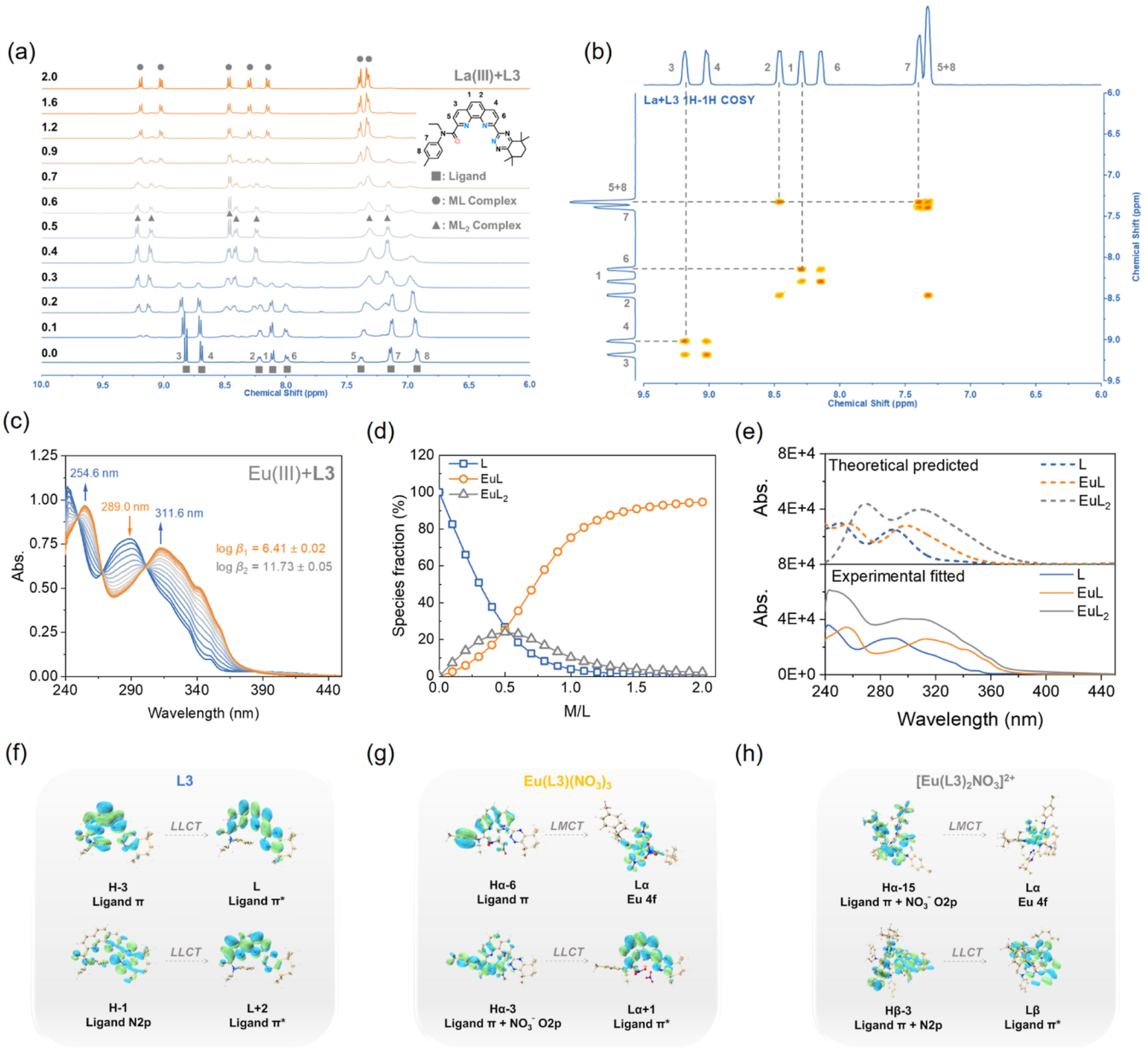

Figure 5. (a) Stacked ^{1}H NMR titration spectra of La(III) and **L3** (■ = ligand peaks; ● = 1:1 complex peaks; ▲ = 1:2 complex peaks); (b) ^{1}H−^{1}H COSY NMR spectra of La(III) and the **L3** complex; (c) UV−vis spectra; (d) species fraction with increasing equivalents of Eu(III) with **L3** during UV−vis spectroscopic titration; (e) TDDFT/PBE0 simulated and experimental UV−vis spectra of **L3**, Eu(**L3**)$(NO_3)_3$, and $[Eu(\mathbf{L3})_2NO_3]^{2+}$. The calculated spectra were blue-shifted by 2229 cm^{-1} to align with the experimental spectra. (f) **L3**, (g) Eu(**L3**)$(NO_3)_3$, and (h) $[Eu(\mathbf{L3})_2NO_3]^{2+}$ associated with electronic transitions.

disadvantages with this direct grafting method, e.g., poor reaction selectivity, easy decomposition of intermediates, and a low yield of end products. In particular, it is difficult to construct unsymmetrical extractants.

In this work, the phenanthroline skeleton in the **L3** extractant was readily afforded using a Friedländer reaction between intermediate **1** and intermediate **2** in one step with high efficiency, proving an effective approach for constructing phenanthroline-derived derivatives. Due to its universality and versatility, a vast number of phenanthroline-based extractants with different structures can be modularly constructed by changing the structure of intermediates **1**, **2**, and **5**, thus providing a solution for the development of highly efficient extractants.

3.3. Extraction and Separation Performance

Initially, ^{241}Am(III) and ^{152,154}Eu(III) served as representative species for An(III) and Ln(III), respectively, to assess the extraction and separation performances of the extractants. As anticipated, the **L3** extractant exhibits outstanding extraction and separation capabilities for Am(III)/Eu(III) across a wide acidity range with $D_{Am(III)}$ = 28−44 and $SF_{Am(III)/Eu(III)}$ = 51−57 (Figure 4c). The peak distribution ratios for Am(III) and Eu(III) are attained at 2 M HNO_3. Compared to **L1** and **L2** (Figure 4a,b), **L3** obviously exhibits a stronger extraction affinity toward Am(III) (**L3** > **L1** > **L2**).

The Am(III)/Eu(III) separation ability follows the order **L3** > **L2** > **L1** and indicates that the separation ability of **L2** and **L3** extractants with bipyridine and phenanthroline skeletons can be improved with an increasing number of N donor atoms. These

https://doi.org/10.1021/jacsau.4c00684
JACS Au 2024, 4, 4744−4756

experimental results are exciting. The trend in separation capabilities of the three ligands observed in the experiments aligns perfectly with our previous theoretical predictions. This not only validates our theoretical model but also strengthens our confidence in the computational methods. Although there are minor deviations in the computational predictions of the extraction trends, we believe that these may be attributed to the diversity of the extracted species. Such a superior performance of **L3** stems from the preorganized phenanthroline skeleton, which maintains the extractant configuration and prevents conformational reversal during metal ion coordination. Additionally, the presence of the electron-rich O donor atom in the amide side chain enhances the extraction capability, while the softer N donor atom in the triazine side chain significantly improves Am(III)/Eu(III) selectivity. These three factors synergistically boost the extraction and separation effects of the **L3** extractant for Am(III)/Eu(III).

Besides Eu(III), the spent fuel solution contains other Ln(III) elements such as Gd(III) and Sm(III), requiring proper separation alongside Eu(III). Remarkably, the **L3** extractant exhibits very weak extraction across the Ln series, implying exceptional group selectivity for An(III) over Ln(III). The $D_{Ln(III)}$ values with an initial Ln concentration of 0.1 mM do not exceed 0.2 at 1−2 M HNO_3 and even fall below 0.1 under the highly acidic condition of 4 M HNO_3, achieving an extremely high $SF_{Am(III)/Ln(III)}$ (Figure 4d and Table S9). The **L3** extractant overcomes the common issue of strong coextraction of light Ln(III) by DAPhen extractants, facilitating complete separation between An(III) and Ln(III).[26]

The slope analysis method was utilized to determine the stoichiometry of the extracted complex. Fittings for Am(III) and Eu(III) extraction by **L3** yield values of 1.84 and 1.45, respectively (Figure 4e), indicating the potential involvement of both ML and ML_2 types of complexes during the extraction. In addition, the proportion of the ML_2-type complex formed between **L3** and Am(III) is higher than that with Eu(III). This disparity may be attributed to the stronger binding affinity of **L3** to Am(III) as compared to that of Eu(III), leading multiple extractants to coordinate with Am(III) preferentially.

In practical application, dilute nitric acid is favored as a stripping agent due to its low cost, easy preparation, and lack of interfering ions. The **L3** extractant was tested using dilute nitric acid of varying concentrations to assess Am(III) stripping efficiency (Figure 4f). Remarkably, lower nitric acid concentrations significantly enhance the stripping efficiency, consistent with the extraction trend. By employing 0.001 M HNO_3 as the stripping agent, the cumulative three-stage stripping efficiency of **L3** reaches 92.72%. It is anticipated that employing more stages would yield a higher stripping efficiency. For BTPhen extractants, water-soluble ligands such as TEDGA need to be used as the stripping agent to achieve similar stripping effects, which undoubtedly increases the difficulty of the operation process and subsequent treatment.[79]

To facilitate the next-generation development of a practical An(III)/Ln(III) separation process, we propose that the **L3** extractant addresses several critical considerations in this field. Specifically, the extractant should exhibit robust capabilities for the extraction of Am(III) and subsequent separation of Am(III) from Ln(III) ions. Moreover, it is essential that the extractant does not extract Ln(III) ions over a wide range of acidities. Furthermore, the target Am(III) ions should be efficiently stripped using dilute nitric acid as the stripping agent. Given that the **L3** extractant is the only known candidate of phenanthroline-derived extractants that is capable of simultaneously fulfilling these requirements, we assert that it holds significant application value and represents a pivotal choice for the advancement of An(III)/Ln(III) separation processes in the future.

3.4. Coordination Modes in the Solution System

Slope analysis reveals that **L3** can generate two complexes, M/L = 1:1 and 1:2 with Am(III) and Eu(III), which is well supported by ^{1}H NMR titration.[80] A comprehensive analysis of Figures 5a and S32 indicates that the peak intensity in the aromatic region of **L3** gradually diminishes with Ln(III) addition. New peaks (▲) continuously emerge, with the intensity peaking in the M/L = 0.4−0.5 range, indicating the initial formation of the ML_2 complex. With further Ln(III) addition, the ML_2 complex peak diminishes and is replaced by a peak group (●) representing the ML complex dominant at M/L = 2.0.

Two-dimensional NMR analysis (^{1}H−^{1}H COSY and ^{1}H−^{1}H NOESY) of the La(III)-**L3** system at the titration end point reveals the coupling relationship of adjacent hydrogen atoms in the formed complexes and the spatial interaction between them. Figure 5b shows that the chemical shifts of benzyl hydrogen (no. 7 and no. 8) in **L3** are similar after coordination, which proves that the electron cloud density on the benzene ring is reduced and the coupling effect is stronger. The ^{1}H−^{1}H NOSEY spectrum contains no cross-peaks beyond the diagonal, indicating the absence of adjacent hydrogen atoms less than 4.5 Å apart (Figure S33). This shows that the complex is uniformly dispersed in the solution system and that there is no agglomeration behavior caused by hydrogen bonding and charge attraction.

The mass spectrometry study further confirmed that Eu(III) and **L3** can form a variety of complexes with stoichiometric ratios of 1:1 and 1:2 in the gas phase, including $[Eu(\mathbf{L3})(NO_3)_2]^+$, $[Eu(\mathbf{L3})_2(NO_3)]^{2+}$, and $[Eu(\mathbf{L3})_2(NO_3)_2]^+$ (Figure S34). The UV−vis absorption spectra of the solution coordination system involving Ln(III) and **L3** were recorded using a UV−vis spectrophotometer and analyzed using the *HypeSpec* program, generating information such as coordination species, stability constants, and species fraction curves throughout the coordination process.[71,81] Due to the presence of aromatic color groups (phenanthroline, triazine, and tolyl), **L3** exhibits distinct absorption spectra in the UV region, allowing Eu(III) to be used as a titrant for studying their coordination mode and ability. Figure 5c shows that with the continuous addition of Eu(III), the absorption peak of **L3** at 289.0 nm gradually decreases and is replaced by two new absorption peaks at 254.6 and 311.6 nm. Fitting the data gave log β values of 6.66 and 11.73 for the $Eu(\mathbf{L3})^{3+}$ and $Eu(\mathbf{L3})_2^{3+}$ complexes, respectively (Figure 5d and Table S15). Eu(III) and **L3** can simultaneously form ML and ML_2 complexes, indicating a positive correlation between molar absorbance of complexes and the number of participating ligands in the coordination process (Figure 5e).

To further understand the nature and causes of the trend in spectral peak changes observed in the experiments, TDDFT calculations were performed for **L3**, Eu**L3**$(NO_3)_3$, and $[Eu(\mathbf{L3})_2NO_3]^{2+}$, all of which have available experimental UV−vis spectral data (Figures S35−S37 and Tables S10−S12). The simulated UV−vis spectra are consistent with the trend observed in the UV−vis titration experiments; that is, the absorption peaks of the complexes show a slight red shift when compared to those of the free ligands (Figure 5e). Moreover, this

https://doi.org/10.1021/jacsau.4c00684
JACS Au 2024, 4, 4744−4756

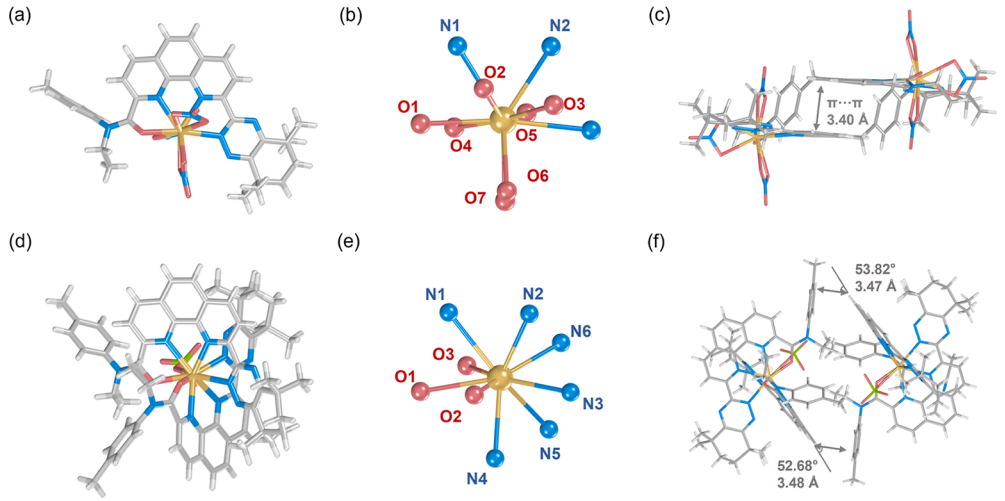

Figure 6. (a) Single-crystal structure, (b) coordination mode of Eu(III) ion, and (c) stacking mode of the Eu(**L3**)$(NO_3)_3$ complex, (d) single-crystal structure, (e) coordination mode of Eu(III) ions, and (f) stacking mode of the $[Eu(\mathbf{L3})_2(ClO_4)](ClO_4)_2$ complex.

red shift trend becomes more pronounced as the coordinated number of ligands increases. Further analyses of electronic transitions reveal that, in addition to ligand-to-ligand charge transfer (LLCT), the intense transitions in the complexes can also be assigned to ligand-to-metal charge transfer (LMCT), i.e., ligand → 4f, when compared to the free ligand. These LMCT transitions are likely the reason for the red shift in absorption peaks (Figure 5f–h). Additionally, the UV–vis spectra for the corresponding Am(III) complexes were also calculated to compare with those of Eu(III) complexes (Figures S38 and S41 and Tables S13 and S14). The results show that the spectra of Am(III) complexes display a slight red shift and the intense transitions associated with the metal can be assigned to LMCT, i.e., ligand → 5f, and metal-to-ligand charge transfer (MLCT), i.e., 5f → ligand. However, within the same spectral energy range, there are no transitions from 4f → ligand in Eu(III) complexes. This is due to the energy of the occupied 4f orbitals being much lower than that of the 5f orbitals, which means transitions from the 4f orbitals to the ligand orbitals require more energy. These computational results reveal the distinct behaviors of the 5f and 4f orbitals during electron transitions and further validate the conclusions drawn from the experimental spectra.

The photoluminescence property of Eu(III) in solution enables the investigation of its photoluminescence characteristics during coordination reactions with ligands, shedding light on coordination thermodynamics and the complex structure.[82] Each peak in the photoluminescence spectrum corresponds to an electron transition of Eu(III) (594 nm, $^5D_0 \rightarrow {}^7F_1$; 616 nm, $^5D_0 \rightarrow 7F_2$; 650 nm, $^5D_0 \rightarrow {}^7F_3$; 683 and 704 nm, $^5D_0 \rightarrow {}^7F_4$). Unlike other phenanthroline-based extractants, the addition of **L3** decreases the photoluminescence intensity of Eu(III) (Figure S42).[83] This may be attributed to the significant difference between the trilinear-state energy level of the phenanthroline skeleton and triazine side chains and the $^5D_0$ level of rare earth, preventing energy conversion to Eu(III). By fitting the photoluminescence data, the stability constants (log β) of the complexes formed by **L3** and Eu(III), Eu(**L3**) and Eu$(\mathbf{L3})_2$, were determined as 6.61 and 11.87, respectively, which are well consistent with the values obtained by UV–vis absorption spectroscopy (Table S15).

3.5. Crystal Structures of Complexes in the Solid State

X-ray single-crystal diffraction is considered as an efficient method for obtaining the structural information on ligands and complexes in the solid phase. Crystals of complexes with different stoichiometries of **L3** and Eu(III) were obtained, and their structures, coordination modes, and packing patterns are depicted in Figure 6, with average bond lengths shown in Table S16. Crystals of two distinct complexes for Eu(III) and **L3**, Eu(**L3**)$(NO_3)_3$ and $[Eu(\mathbf{L3})_2(ClO_4)](ClO_4)_2$, were obtained through a solvent diffusion method.

Different from $CyMe_4$-BTPhen extractants, the triazine side chain configuration of **L3** involved in coordination is the same as that of the ligand crystal, which avoids the energy barrier required to overcome due to the conformation inversion of the ligand during coordination.[19] In both complexes, **L3** engages in coordination with Eu(III) ions in a tetradentate chelating manner.[84] However, the coordination patterns differ noticeably. In Eu(**L3**)$(NO_3)_3$, the phenanthroline skeleton in **L3** flips to the same side when coordinating with Eu(III), with its two N donor atoms on the phenanthroline skeleton alongside the triazine (N)/amide (O) side chains participating in coordination (Figure 6a). Concurrently, three nitrate ions coordinate with Eu(III) in a bidentate mode, providing additional coordination atoms while neutralizing the positive charge of the complex (Figure 6b). Ten donor atoms coordinate with Eu(III) simultaneously, showing slight differences in average bond lengths: Eu–O(amide)(2.42 Å) < Eu–O(NO_3^-)(2.50 Å) < Eu–N(phen)(2.56 Å) ≈ Eu–N(triazine)(2.57 Å) (Table S16). Figure 6c illustrates that the distance between phenanthroline skeletons in two near complexes is 3.40 Å, leading to a relatively strong π–π stacking interaction.[85]

Conversely, when the anion is the weaker coordinating ClO_4^-, the second **L3** ligand can readily participate in coordination (Figure 6d), which is similar to the tetradentate phenanthroline-derived phosphonate ligands.[86] Only one ClO_4^- atom acts as an ancillary ligand for coordination and charge neutralization, with the remaining charge being balanced by free ClO_4^- anions. In $[Eu(\mathbf{L3})_2(ClO_4)](ClO_4)_2$, Eu(III) exhibits a coordination number of 9, contributed by two **L3** ligands and one ClO_4^- ligand (Figure 6e). This could be attributed to the larger volume of ClO_4^-, hindering the formation of a 10-coordinate complex. However, due to the larger volume of $[Eu(\mathbf{L3})_2(ClO_4)]$-

https://doi.org/10.1021/jacsau.4c00684
JACS Au 2024, 4, 4744–4756

$(ClO_4)_2$, it cannot form extensive offset face-to-face $\pi-\pi$ interactions, relying instead on tilted edge-to-face $\pi-\pi$ interactions between the phenanthroline and toluene moieties on the side chain of another ligand (Figure 6f). The further comparison of the crystallographic bond lengths with the theoretically predicted ones gives a discrepancy of less than 3% between them (Table S16), again confirming the accuracy of our theoretical methods and models used.

Given the unavailability of a single-crystal structure of 1:2 complex of **L3** in nitric acid solution, we performed DFT calculations on the $[M(\mathbf{L3})_2NO_3]^{2+}$ [M = Am(III), Eu(III)] complexes to gain detailed structural insights on the molecular level (Figures S43−S45 and Tables S19 and S20). In these optimized complexes, two **L3** molecules coordinate with Am(III)/Eu(III) in a tetradentate chelate form, complemented by an additional nitrate anion participating as a bidentate ligand, yielding a coordination number of 10.

4. CONCLUSIONS

In summary, to overcome the inherent limitations of existing An(III)/Ln(III) separation extractants in simultaneously achieving extraction, separation, and stripping performances, we employed DFT calculations to assist in screening out a novel unsymmetrical phen-derived extractant with potential An(III)/Ln(III) separation capabilities. Subsequently, a *de novo* synthetic approach was developed to efficiently construct this optimal extractant with a preorganized phenanthroline skeleton. Due to its universality and versatility, a vast amount of phenanthroline-based extractants with desired structures could be modularly constructed by simply adjusting the structure of intermediates, thus providing an effective solution for the development of highly efficient extractants. As anticipated by DFT results, the Et-Tol-CyMe$_4$-ATPhen (**L3**) extractant demonstrated a preferential extraction of Am(III) over Ln(III), achieving a high Am(III)/Ln(III) separation factor ($D_{Am} > 40$, $SF_{Am(III)/Ln(III)} > 280$). Meanwhile, Am(III) could be easily stripped using the most convenient dilute nitric acid as the stripping agent. The systematic spectroscopic analysis using ^{1}H NMR, ESI-MS, UV−vis absorption, and photoluminescence spectroscopy elucidated that Et-Tol-CyMe$_4$-ATPhen coordinates with Ln(III) in two complexes with $\log \beta_1 = 6.41 \pm 0.02$ and $\log \beta_2 = 11.73 \pm 0.05$. Finally, single-crystal structures of Eu(III) complexes with different stoichiometric ratios $(Eu(\mathbf{L3})(NO_3)_3$ and $[Eu(\mathbf{L3})_2(ClO_4)](ClO_4)_2)$ facilitated a molecule-level understanding of the coordination mode of **L3** with f-block elements. The unsymmetrical extractant developed in this work holds the capability required to discern subtle chemical distinctions between An(III) and Ln(III), overcoming the current challenges in An(III)/Ln(III) separation. Consequently, this work provides an ideal candidate for a next-generation extractant in An(III)/Ln(III) separation.

■ ASSOCIATED CONTENT

Supporting Information

The Supporting Information is available free of charge at https://pubs.acs.org/doi/10.1021/jacsau.4c00684.

Additional experimental methods and results, DFT calculation results, and organic synthesis results (NMR, ESI-MS, and organic element analysis) (PDF)

Crystallographic data for **L3** (CIF)

Crystallographic data for $(Eu(\mathbf{L3})(NO_3)_3$ (CIF)

Crystallographic data for $[Eu(\mathbf{L3})_2(ClO_4)](ClO_4)_2)$ (CIF)

■ AUTHOR INFORMATION

Corresponding Authors

Jing Su − *College of Chemistry, Sichuan University, Chengdu 610064, China;* orcid.org/0000-0002-6895-2150; Email: jingsu@scu.edu.cn

Chao Xu − *Institute of Nuclear and New Energy Technology, Tsinghua University, Beijing 100084, China;* orcid.org/0000-0001-5539-4754; Email: xuchao@tsinghua.edu.cn

Chengliang Xiao − *College of Chemical and Biological Engineering, Zhejiang University, Hangzhou 310058, China; Institute of Zhejiang University-Quzhou, Quzhou 324000, China;* orcid.org/0000-0001-5081-2398; Email: xiaoc@zju.edu.cn

Authors

Xiaofan Yang − *College of Chemical and Biological Engineering, Zhejiang University, Hangzhou 310058, China;* orcid.org/0000-0002-4916-7050

Dong Fang − *College of Chemical and Biological Engineering, Zhejiang University, Hangzhou 310058, China; Institute of Zhejiang University-Quzhou, Quzhou 324000, China*

Linjia Chen − *College of Chemistry, Sichuan University, Chengdu 610064, China*

Yaoyang Liu − *Institute of Nuclear and New Energy Technology, Tsinghua University, Beijing 100084, China*

Shihui Wang − *College of Chemical and Biological Engineering, Zhejiang University, Hangzhou 310058, China*

Lei Xu − *Institute of Nuclear-Agricultural Science, Key Laboratory of Nuclear Agricultural Sciences of Ministry of Agriculture and Zhejiang Province, Zhejiang University, Hangzhou 310058, China*

Anyun Zhang − *College of Chemical and Biological Engineering, Zhejiang University, Hangzhou 310058, China;* orcid.org/0000-0001-5816-3812

Complete contact information is available at: https://pubs.acs.org/10.1021/jacsau.4c00684

Author Contributions

[#]The first three authors contributed equally: X.Y., D.F., and L.C. **Xiaofan Yang:** conceptualization, investigation, writing—original draft; **Dong Fang:** resources, methodology; **Linjia Chen:** performed and analysed all theoretical work, writing—original draft; **Yaoyang Liu:** resources; **Shihui Wang**: visualization; **Lei Xu**: validation; **Anyun Zhang**: project administration; **Jing Su:** performed and analysed all theoretical work, writing—review and editing, funding acquisition; **Chao Xu:** funding acquisition, writing—review and editing; **Chengliang Xiao**: funding acquisition, supervision, writing-review and editing.

Notes

The authors declare no competing financial interest.

The research presented in this article was posted on a preprint server prior to publication. The corresponding preprint article can be found here (DOI: https://doi.org/10.21203/rs.3.rs-4355272/v1).

■ ACKNOWLEDGMENTS

We are grateful for financial support from the National Natural Science Foundation of China (**U2067213**, **22076130**, **22206168**, and **22325603**). Thanks to Dr. Jiyong Liu of the Department of Chemistry and Dr. Xiaoyan Xiao of the School of Materials Science and Engineering, Zhejiang University, for their help in single-crystal experiments.

■ REFERENCES

(1) Albrecht-Schmitt, T. E. Actinide Chemistry at the Extreme. *Inorg. Chem.* **2019**, *58*, 1721−1723.
(2) Voncken, J. H. L. *Physical and Chemical Properties of the Rare Earths*; Voncken, J. H. L., Ed.; Springer International Publishing: Cham, 2016.
(3) Szabo, Z.; Toraishi, T.; Vallet, V.; Grenthe, I. Solution coordination chemistry of actinides: Thermodynamics, structure and reaction mechanisms. *Coord. Chem. Rev.* **2006**, *250*, 784−815.
(4) Edelstein, N. M.; Fuger, J.; Katz, J. J.; Morss, L. R. *Summary and Comparison of Properties of the Actinide and Transactinide Elements*; Morss, L. R.; Edelstein, N. M.; Fuger, J., Eds.; Springer Netherlands: Dordrecht, 2011.
(5) Galley, S. S.; Pattenaude, S. A.; Gaggioli, C. A.; Qiao, Y.; Sperling, J. M.; Zeller, M.; Pakhira, S.; Mendoza-Cortes, J. L.; Schelter, E. J.; Albrecht-Schmitt, T. E.; et al. Synthesis and Characterization of Tris-chelate Complexes for Understanding f-Orbital Bonding in Later Actinides. *J. Am. Chem. Soc.* **2019**, *141*, 2356−2366.
(6) Salvatores, M.; Palmiotti, G. Radioactive waste partitioning and transmutation within advanced fuel cycles: Achievements and challenges. *Prog. Part. Nucl. Phys.* **2011**, *66*, 144−166.
(7) Xiao, C.; Hassanzadeh Fard, Z.; Sarma, D.; Song, T.; Xu, C.; Kanatzidis, M. G. Highly Efficient Separation of Trivalent Minor Actinides by a Layered Metal Sulfide ($KInSn_2S_6$) from Acidic Radioactive Waste. *J. Am. Chem. Soc.* **2017**, *139*, 16494−16497.
(8) Chadwick, M. B.; Herman, M.; Obložinský, P.; Dunn, M. E.; Danon, Y.; Kahler, A. C.; Smith, D. L.; Pritychenko, B.; Arbanas, G.; et al. ENDF/B-VII.1 Nuclear Data for Science and Technology: Cross Sections, Covariances, Fission Product Yields and Decay Data. *Nucl. Data Sheets* **2011**, *112*, 2887−2996.
(9) Zhang, H.; Li, A.; Li, K.; Wang, Z.; Xu, X.; Wang, Y.; Sheridan, M. V.; Hu, H.; Xu, C.; Alekseev, E. V.; et al. Ultrafiltration separation of Am(VI)-polyoxometalate from lanthanides. *Nature* **2023**, *616*, 482−487.
(10) Wang, Z.; Lu, J.; Dong, X.; Yan, Q.; Feng, X.; Hu, H.; Wang, S.; Chen, J.; Li, J.; Xu, C. Ultra-Efficient Americium/Lanthanide Separation through Oxidation State Control. *J. Am. Chem. Soc.* **2022**, *144*, 6383−6389.
(11) Leoncini, A.; Huskens, J.; Verboom, W. Ligands for f-element extraction used in the nuclear fuel cycle. *Chem. Soc. Rev.* **2017**, *46*, 7229−7273.
(12) Klopman, G. Chemical reactivity and the concept of charge- and frontier-controlled reactions. *J. Am. Chem. Soc.* **1968**, *90*, 223−234.
(13) Parr, R. G.; Pearson, R. G. Absolute hardness: companion parameter to absolute electronegativity. *J. Am. Chem. Soc.* **1983**, *105*, 7512−7516.
(14) Bessen, N. P.; Jackson, J. A.; Jensen, M. P.; Shafer, J. C. Sulfur donating extractants for the separation of trivalent actinides and lanthanides. *Coord. Chem. Rev.* **2020**, *421*, 213446.
(15) Kolarik, Z.; Müllich, U.; Gassner, F. Selective Extraction of Am(III) over Eu(III) by 2,6-Ditriazolyl- and 2,6-Ditriazinylpyridines. *Solvent Extr. Ion Exch.* **1999**, *17*, 23−32.
(16) Panak, P. J.; Geist, A. Complexation and Extraction of Trivalent Actinides and Lanthanides by Triazinylpyridine N-Donor Ligands. *Chem. Rev.* **2013**, *113*, 1199−1236.
(17) Geist, A.; Hill, C.; Modolo, G.; Foreman, M. R. S. J.; Weigl, M.; Gompper, K.; Hudson, M. J. 6,6′-Bis(5,5,8,8-tetramethyl-5,6,7,8-tetrahydro-benzo[1,2,4]triazin-3-yl) [2,2′]bipyridine, an Effective Extracting Agent for the Separation of Americium(III) and Curium(III) from the Lanthanides. *Solvent Extr. Ion Exch.* **2006**, *24*, 463−483.
(18) Lewis, F. W.; Harwood, L. M.; Hudson, M. J.; Drew, M. G. B.; Hubscher-Bruder, V.; Videva, V.; Arnaud-Neu, F.; Stamberg, K.; Vyas, S. BTBPs versus BTPhens: Some Reasons for Their Differences in Properties Concerning the Partitioning of Minor Actinides and the Advantages of BTPhens. *Inorg. Chem.* **2013**, *52*, 4993−5005.
(19) Lewis, F. W.; Harwood, L. M.; Hudson, M. J.; Drew, M. G. B.; Desreux, J. F.; Vidick, G.; Bouslimani, N.; Modolo, G.; Wilden, A.; Sypula, M.; et al. Highly Efficient Separation of Actinides from Lanthanides by a Phenanthroline-Derived Bis-triazine Ligand. *J. Am. Chem. Soc.* **2011**, *133*, 13093−13102.
(20) Geist, A.; Panak, P. J. Recent Progress in Trivalent Actinide and Lanthanide Solvent Extraction and Coordination Chemistry with Triazinylpyridine N Donor Ligands. *Solvent Extr. Ion Exch.* **2021**, *39*, 128−151.
(21) Merrill, D.; Hancock, R. D. Metal ion selectivities of the highly preorganized tetradentate ligand 1,10-phenanthroline-2,9-dicarboxamide with lanthanide(III) ions and some actinide ions. *Radiochim. Acta* **2011**, *99*, 161−166.
(22) Xu, L.; Yang, X.; Zhang, A.; Xu, C.; Xiao, C. Separation and complexation of f-block elements using hard-soft donors combined phenanthroline extractants. *Coord. Chem. Rev.* **2023**, *496*, 215404.
(23) Xiao, C.; Wang, C.; Yuan, L.; Li, B.; He, H.; Wang, S.; Zhao, Y.; Chai, Z.; Shi, W. Excellent Selectivity for Actinides with a Tetradentate 2,9-Diamide-1,10-Phenanthroline Ligand in Highly Acidic Solution: A Hard−Soft Donor Combined Strategy. *Inorg. Chem.* **2014**, *53*, 1712−1720.
(24) Zhang, X.; Yuan, L.; Chai, Z.; Shi, W. A new solvent system containing N,N′-diethyl-N,N′-ditolyl-2,9-diamide-1,10-phenanthroline in 1-(trifluoromethyl)-3-nitrobenzene for highly selective UO_2^{2+} extraction. *Sep. Purif. Technol.* **2016**, *168*, 232−237.
(25) Zhang, X.; Wu, Q.; Lan, J.; Yuan, L.; Xu, C.; Chai, Z.; Shi, W. Highly selective extraction of Pu (IV) and Am (III) by N,N′-diethyl-N,N′-ditolyl-2,9-diamide-1,10-phenanthroline ligand: An experimental and theoretical study. *Sep. Purif. Technol.* **2019**, *223*, 274−281.
(26) Yang, X.; Ren, P.; Yang, Q.; Geng, J.; Zhang, J.; Yuan, L.; Tang, H.; Chai, Z.; Shi, W. Strong Periodic Tendency of Trivalent Lanthanides Coordinated with a Phenanthroline-Based Ligand: Cascade Countercurrent Extraction, Spectroscopy, and Crystallography. *Inorg. Chem.* **2021**, *60*, 9745−9756.
(27) Jansone-Popova, S.; Ivanov, A. S.; Bryantsev, V. S.; Sloop, F. V.; Custelcean, R.; Popovs, I.; Dekarske, M. M.; Moyer, B. A. Bis-lactam-1,10-phenanthroline (BLPhen), a New Type of Preorganized Mixed N,O-Donor Ligand That Separates Am(III) over Eu(III) with Exceptionally High Efficiency. *Inorg. Chem.* **2017**, *56*, 5911−5917.
(28) Pramanik, S.; Li, B.; Driscoll, D. M.; Johnson, K. R.; Evans, B. R.; Damron, J. T.; Ivanov, A. S.; Jiang, D.-e.; Einkauf, J.; Popovs, I.; Jansone-Popova, S.; et al. Tetradentate Ligand's Chameleon-Like Behavior Offers Recognition of Specific Lanthanides. *J. Am. Chem. Soc.* **2024**, *146*, 25669−25679.
(29) Healy, M. R.; Ivanov, A. S.; Karslyan, Y.; Bryantsev, V. S.; Moyer, B. A.; Jansone Popova, S. Efficient Separation of Light Lanthanides(III) by Using Bis-Lactam Phenanthroline Ligands. *Chem.—Eur. J.* **2019**, *25*, 6326−6331.
(30) Hudson, M. J.; Harwood, L. M.; Laventine, D. M.; Lewis, F. W. Use of Soft Heterocyclic N-Donor Ligands To Separate Actinides and Lanthanides. *Inorg. Chem.* **2013**, *52*, 3414−3428.
(31) Archer, E. M.; Galley, S. S.; Jackson, J. A.; Shafer, J. C. Investigation of f-Element Interactions with Functionalized Diamides of Phenanthroline-Based Ligands. *Solvent Extr. Ion Exch.* **2023**, *41*, 697−740.
(32) Macerata, E.; Mossini, E.; Scaravaggi, S.; Mariani, M.; Mele, A.; Panzeri, W.; Boubals, N.; Berthon, L.; Charbonnel, M.; Sansone, F.; et al. Hydrophilic Clicked 2,6-Bis-triazolyl-pyridines Endowed with High Actinide Selectivity and Radiochemical Stability: Toward a Closed Nuclear Fuel Cycle. *J. Am. Chem. Soc.* **2016**, *138*, 7232−7235.
(33) Higginson, M. A.; Kyle, N. D.; Marsden, O. J.; Thompson, P.; Livens, F. R.; Heath, S. L. Synthesis of functionalised BTPhen derivatives − effects on solubility and americium extraction. *Dalton Trans.* **2015**, *44*, 16547−16552.

https://doi.org/10.1021/jacsau.4c00684
JACS Au 2024, 4, 4744−4756

(34) Edwards, A. C.; Geist, A.; Müllich, U.; Sharrad, C. A.; Pritchard, R. G.; Whitehead, R. C.; Harwood, L. M. Transition metal-free, visible-light mediated synthesis of 1,10-phenanthroline derived ligand systems. *Chem. Commun.* **2017**, *53*, 8160−8163.
(35) Yang, X.; Xu, L.; Fang, D.; Zhang, A.; Xiao, C. Progress in phenanthroline-derived extractants for trivalent actinides and lanthanides separation: where to next? *Chem. Commun.* **2024**.
(36) Lehman-Andino, I.; Su, J.; Papathanasiou, K. E.; Eaton, T. M.; Jian, J.; Dan, D.; Albrecht-Schmitt, T. E.; Dares, C. J.; Batista, E. R.; Yang, P.; et al. Soft-donor dipicolinamide derivatives for selective actinide(III)/lanthanide(III) separation: the role of S- vs. O-donor sites. *Chem. Commun.* **2019**, *55*, 2441−2444.
(37) Lan, J.; Shi, W.; Yuan, L.; Li, J.; Zhao, Y.; Chai, Z. Recent advances in computational modeling and simulations on the An(III)/Ln(III) separation process. *Coord. Chem. Rev.* **2012**, *256*, 1406−1417.
(38) Su, L.; Wu, Q.; Wang, C.; Lan, J.; Shi, W. Heterocyclic Ligands with Different N/O Donor Modes for Am(III)/Eu(III) Separation: A Theoretical Perspective. *Inorg. Chem.* **2024**, *63*, 9478−9486.
(39) Daly, S. R.; Keith, J. M.; Batista, E. R.; Boland, K. S.; Clark, D. L.; Kozimor, S. A.; Martin, R. L. Sulfur K-edge X-ray Absorption Spectroscopy and Time-Dependent Density Functional Theory of Dithiophosphinate Extractants: Minor Actinide Selectivity and Electronic Structure Correlations. *J. Am. Chem. Soc.* **2012**, *134*, 14408−14422.
(40) Goodwin, C. A. P.; Schlimgen, A. W.; Albrecht-Schönzart, T. E.; Batista, E. R.; Gaunt, A. J.; Janicke, M. T.; Kozimor, S. A.; Scott, B. L.; Stevens, L. M.; White, F. D.; et al. Structural and Spectroscopic Comparison of Soft-Se vs. Hard-O Donor Bonding in Trivalent Americium/Neodymium Molecules. *Angew. Chem., Int. Ed.* **2021**, *60*, 9459−9466.
(41) Chen, B.; Hong, S.; Dai, X.; Li, X.; Huang, Q.; Sun, T.; Cao, D.; Zhang, H.; Chai, Z.; Diwu, J.; et al. In Vivo Uranium Decorporation by a Tailor-Made Hexadentate Ligand. *J. Am. Chem. Soc.* **2022**, *144*, 11054−11058.
(42) Zhang, X.; Adelman, S. L.; Arko, B. T.; De Silva, C. R.; Su, J.; Kozimor, S. A.; Mocko, V.; Shafer, J. C.; Stein, B. W.; Schreckenbach, G.; et al. Advancing the Am Extractant Design through the Interplay among Planarity, Preorganization, and Substitution Effects. *Inorg. Chem.* **2022**, *61*, 11556−11570.
(43) Kelley, M. P.; Su, J.; Urban, M.; Luckey, M.; Batista, E. R.; Yang, P.; Shafer, J. C. On the Origin of Covalent Bonding in Heavy Actinides. *J. Am. Chem. Soc.* **2017**, *139*, 9901−9908.
(44) Gannon, A.; Marxsen, S.; Mueller, K.; Quaife, B. D.; Mendoza-Cortes, J. L. Using a High-Throughput Screening Algorithm and relativistic Density Functional Theory to Find Chelating Agents for Separation of Radioactive Waste. *arXiv* **2018**, arXiv:1806.09733 Preprint.
(45) Zapata-Escobar, A. D.; Pakhira, S.; Barroso-Flores, J.; Aucar, G. A.; Mendoza-Cortes, J. L. Relativistic quantum calculations to understand the contribution of f-type atomic orbitals and chemical bonding of actinides with organic ligands. *Phys. Chem. Chem. Phys.* **2023**, *25*, 5592−5601.
(46) Hohenberg, P.; Kohn, W. Inhomogeneous Electron Gas. *Phys. Rev.* **1964**, *136*, B864−B871.
(47) Kohn, W.; Sham, L. J. Self-Consistent Equations Including Exchange and Correlation Effects. *Phys. Rev.* **1965**, *140*, A1133−A1138.
(48) Adamo, C.; Barone, V. Toward reliable density functional methods without adjustable parameters: The PBE0 model. *J. Chem. Phys.* **1999**, *110*, 6158−6170.
(49) Frisch, M. J.; Trucks, G. W.; Schlegel, H. B.; Scuseria, G. E.; Robb, M. A.; Cheeseman, J. R.; Scalmani, G.; Barone, V.; Petersson, G. A.; Nakatsuji, H.; et al. *Gaussian 16*; Wallingford: CT, 2016.
(50) Cao, X.; Dolg, M. Segmented contraction scheme for small-core lanthanide pseudopotential basis sets. *J. Mol. Struc. Theochem.* **2002**, *581*, 139−147.
(51) Dolg, M.; Stoll, H.; Preuss, H. Energy-adjusted ab initio pseudopotentials for the rare earth elements. *J. Chem. Phys.* **1989**, *90*, 1730−1734.
(52) Cao, X.; Dolg, M. Segmented contraction scheme for small-core actinide pseudopotential basis sets. *J. Mol. Struc. Theochem.* **2004**, *673*, 203−209.
(53) Cao, X.; Dolg, M.; Stoll, H. Valence basis sets for relativistic energy-consistent small-core actinide pseudopotentials. *J. Chem. Phys.* **2003**, *118*, 487−496.
(54) Weigend, F.; Ahlrichs, R. Balanced basis sets of split valence, triple zeta valence and quadruple zeta valence quality for H to Rn: Design and assessment of accuracy. *Phys. Chem. Chem. Phys.* **2005**, *7*, 3297.
(55) Krishnan, R.; Binkley, J. S.; Seeger, R.; Pople, J. A. Self-consistent molecular orbital methods. XX. A basis set for correlated wave functions. *J. Chem. Phys.* **1980**, *72*, 650−654.
(56) Marenich, A. V.; Cramer, C. J.; Truhlar, D. G. Universal Solvation Model Based on Solute Electron Density and on a Continuum Model of the Solvent Defined by the Bulk Dielectric Constant and Atomic Surface Tensions. *J. Phys. Chem. B* **2009**, *113*, 6378−6396.
(57) Mayer, I. Charge, bond order and valence in the AB initio SCF theory. *Chem. Phys. Lett.* **1983**, *97*, 270−274.
(58) Nalewajski, R. F.; Mrozek, J. Modified valence indices from the two-particle density matrix. *Int. J. Quantum Chem.* **1994**, *51*, 187−200.
(59) Mitoraj, M.; Michalak, A. Natural orbitals for chemical valence as descriptors of chemical bonding in transition metal complexes. *J. Mol. Model.* **2007**, *13*, 347−355.
(60) Ziegler, T.; Rauk, A. On the calculation of bonding energies by the Hartree Fock Slater method. *Theor. Chim. Acta* **1977**, *46*, 1−10.
(61) Bickelhaupt, F. M.; Baerends, E. J. *Kohn-Sham Density Functional Theory: Predicting and Understanding Chemistry*; Lipkowitz, K. B.; Boyd, D. B., Eds.; John Wiley & Sons, Inc: Hoboken, NJ, USA, 2000.
(62) Hopffgarten, M. V.; Frenking, G. Energy decomposition analysis. *WIREs. Comput. Mol. Sci.* **2012**, *2*, 43−62.
(63) Mitoraj, M. P.; Michalak, A.; Ziegler, T. A Combined Charge and Energy Decomposition Scheme for Bond Analysis. *J. Chem. Theory Comput.* **2009**, *5*, 962−975.
(64) Perdew, J. P.; Burke, K.; Ernzerhof, M. Generalized Gradient Approximation Made Simple. *Phys. Rev. Lett.* **1996**, *77*, 3865−3868.
(65) Lenthe, E. V.; Baerends, E. J.; Snijders, J. G. Relativistic regular two-component Hamiltonians. *J. Chem. Phys.* **1993**, *99*, 4597−4610.
(66) Van Lenthe, E.; Baerends, E. J. Optimized Slater-type basis sets for the elements 1−118. *J. Comput. Chem.* **2003**, *24*, 1142−1156.
(67) Te Velde, G.; Bickelhaupt, F. M.; Baerends, E. J.; Fonseca Guerra, C.; van Gisbergen, S. J. A.; Snijders, J. G.; Ziegler, T. Chemistry with ADF. *J. Comput. Chem.* **2001**, *22*, 931−967.
(68) Fonseca Guerra, C.; Snijders, J. G.; Te Velde, G.; Baerends, E. J. Towards an order-N DFT method. *Theor. Chem. Acc.* **1998**, *99*, 391−403.
(69) Hu, S.; Liu, J.; Gibson, J. K.; Li, J. Periodic Trends in Actinyl Thio-Crown Ether Complexes. *Inorg. Chem.* **2018**, *57*, 2899−2907.
(70) Hu, S.; Li, W.; Dong, L.; Gibson, J. K.; Li, J. Crown ether complexes of actinyls: a computational assessment of $AnO_2(15\text{-crown-}5)^{2+}$ (An = U, Np, Pu, Am, Cm). *Dalton Trans.* **2017**, *46*, 12354−12363.
(71) Gans, P.; Sabatini, A.; Vacca, A. Investigation of equilibria in solution. Determination of equilibrium constants with the HYPERQUAD suite of programs. *Talanta* **1996**, *43*, 1739−1753.
(72) Polinski, M. J.; Grant, D. J.; Wang, S.; Alekseev, E. V.; Cross, J. N.; Villa, E. M.; Depmeier, W.; Gagliardi, L.; Albrecht-Schmitt, T. E. Differentiating between Trivalent Lanthanides and Actinides. *J. Am. Chem. Soc.* **2012**, *134*, 10682−10692.
(73) Neidig, M. L.; Clark, D. L.; Martin, R. L. Covalency in f-element complexes. *Coord. Chem. Rev.* **2013**, *257*, 394−406.
(74) Cross, J. N.; Su, J.; Batista, E. R.; Cary, S. K.; Evans, W. J.; Kozimor, S. A.; Mocko, V.; Scott, B. L.; Stein, B. W.; Windorff, C. J.; et al. Covalency in Americium(III) Hexachloride. *J. Am. Chem. Soc.* **2017**, *139*, 8667−8677.
(75) Su, J.; Batista, E. R.; Boland, K. S.; Bone, S. E.; Bradley, J. A.; Cary, S. K.; Clark, D. L.; Conradson, S. D.; Ditter, A. S.; Kaltsoyannis, N.; et al. Energy-Degeneracy-Driven Covalency in Actinide Bonding. *J. Am. Chem. Soc.* **2018**, *140*, 17977−17984.

https://doi.org/10.1021/jacsau.4c00684
JACS Au 2024, 4, 4744−4756

(76) Lu, J.; Cantu, D. C.; Nguyen, M.; Li, J.; Glezakou, V.; Rousseau, R. Norm-Conserving Pseudopotentials and Basis Sets To Explore Lanthanide Chemistry in Complex Environments. *J. Chem. Theory Comput.* **2019**, *15*, 5987−5997.
(77) Lu, J.; Cantu, D. C.; Xu, C.; Nguyen, M.; Hu, H.; Glezakou, V.; Rousseau, R.; Li, J. Norm-Conserving Pseudopotentials and Basis Sets to Explore Actinide Chemistry in Complex Environments. *J. Chem. Theory Comput.* **2021**, *17*, 3360−3371.
(78) Yang, D. X.; Colletti, S. L.; Wu, K.; Song, M.; Li, G. Y.; Shen, H. C. Palladium-Catalyzed Suzuki−Miyaura Coupling of Pyridyl-2-boronic Esters with Aryl Halides Using Highly Active and Air-Stable Phosphine Chloride and Oxide Ligands. *Org. Lett.* **2009**, *11*, 381−384.
(79) Zsabka, P.; Van Hecke, K.; Adriaensen, L.; Wilden, A.; Modolo, G.; Verwerft, M.; Binnemans, K.; Cardinaels, T. Selective extraction of trivalent actinides using $CyMe_4$-BTPhen in the ionic liquid Aliquat-336 nitrate. *RSC Adv.* **2021**, *11*, 6014−6021.
(80) Williamson, M. P. Using chemical shift perturbation to characterise ligand binding. *Prog. Nucl. Magn. Reson. Spectrosc.* **2013**, *73*, 1−16.
(81) Thordarson, P. Determining association constants from titration experiments in supramolecular chemistry. *Chem. Soc. Rev.* **2011**, *40*, 1305−1323.
(82) Binnemans, K. Interpretation of europium(III) spectra. *Coord. Chem. Rev.* **2015**, *295*, 1−45.
(83) Bremer, A.; Whittaker, D. M.; Sharrad, C. A.; Geist, A.; Panak, P. J. Complexation of Cm(III) and Eu(III) with $CyMe_4$-BTPhen and $CyMe_4$-BTBP studied by time resolved laser fluorescence spectroscopy. *Dalton Trans.* **2014**, *43*, 2684−2694.
(84) Whittaker, D. M.; Griffiths, T. L.; Helliwell, M.; Swinburne, A. N.; Natrajan, L. S.; Lewis, F. W.; Harwood, L. M.; Parry, S. A.; Sharrad, C. A. Lanthanide Speciation in Potential SANEX and GANEX Actinide/Lanthanide Separations Using Tetra-N-Donor Extractants. *Inorg. Chem.* **2013**, *52*, 3429−3444.
(85) Główka, M.; Martynowski, D.; Kozłowska, K. Stacking of six-membered aromatic rings in crystals. *J. Mol. Struct.* **1999**, *474*, 81−89.
(86) Yang, X.; Xu, L.; Hao, Y.; Meng, R.; Zhang, X.; Lei, L.; Xiao, C. Effect of Counteranions on the Extraction and Complexation of Trivalent Lanthanides with Tetradentate Phenanthroline-Derived Phosphonate Ligands. *Inorg. Chem.* **2020**, *59*, 17453−17463.

https://doi.org/10.1021/jacsau.4c00684
JACS Au 2024, 4, 4744−4756